FLOW FIELD CHARACTERISTICS IN THE HOUSING OF NONCIRCULAR GEAR FLOWMETER

Lee G. S.* and Park M. Y.
*Author for correspondence
Department of Mechanical and Automotive Engineering,
University of Ulsan,
Ulsan, 680-749,
Korea,
E-mail: gslee@mail.ulsan.ac.kr

ABSTRACT

In order to find the factors which affect the accuracy of the flow rate measurement, the inner flow characteristics of an oval-gear flowmeter were investigated. Inner flow field was analyzed by using the fluid-structure coupling technique with ADINA-FSI (Fluid-Structure Interactions) module. The results were compared with experimental results such as flow visualization and measurements of flow rate, rpm, and pressure drop.

As a result, the pressure on the rotor surface was periodically changed with respect to the rotational angle, from the maximum value of the inlet pressure to the minimum value of the outlet pressure. The rotor tip velocity showed the periodical changes with respect to the rotational angle. The creation, movement, and discharge of vortices were observed by turns around the upper and the lower rotor, which are produced by the rotation of the rotor and the changes in the flow passage area and contour in the housing. Larger pressure difference between the inlet and the exit of the housing showed higher flow rate. The flowmeter used in the present experiment had the precision of 1%, in view of the ppl (pulse per liter) variation as a function of flow rate. The power loss, the difference between the theoretical driving power of the rotor due to the pressure difference and the actual power of the rotor, was increased as the flow rate was increased.

INTRODUCTION

Recent trends towards higher cost of energy such as oil have necessitated not only the development of new energy sources but also more effective use of energy. The exact measurement of flow rate can be such an effective use of energy and is also necessary for fair commercial trade. The major factors to affect the precision of a positive displacement flowmeter are leakage flows through the clearances between the housing and rotors.

In a previous investigation [1], modified equation for leakage flow with respect to variations of fluid viscosity was suggested. Design conditions for elliptic noncircular gear were also studied [2,3]. In spite of necessity of detail information about inner flow field characteristics in such a flowmeter with elliptic rotor, there are few papers.

In the present study, inner flow characteristics of the oval gear flowmeter were examined with aid of ADINA-FSI (Fluid-Structure Interactions). Flow visualization was carried out to compare the results of FSI analysis. In actual flowmeter experiment, revolution per minute (rpm) and pressure difference between the inlet and outlet of the housing were investigated as a function of flow rate. These results were compared each other. Rotor driving power and power loss were roughly analysed with the experimental results and the consideration of pressure distributions around the rotor.

NOMENCLATURE

A	[m^2]	Area
F	[kN]	Force
$\dot{m}$	[kg/s]	Mass flow rate
ΔP	[kPa]	Pressure difference between the inlet and outlet of the housing
ppl	[pulse/litre]	Pulse per litre
Q	[litre/min]	Flow rate
rpm	[rev/min]	Revolution per minute
T	[kN-m]	Torque
$\dot{W}_P$	[Watt]	Rotor driving power by the pressure difference between the inlet and outlet of the housing
$\dot{W}_R$	[Watt]	Actual rotor driving power by the pressure difference considering the long axis of the rotors
$\dot{W}_{RM}$	[Watt]	Modified actual rotor driving power by the pressure around the elliptical surface of rotors

Special characters

ρ	[kg/m^3]	Density of fluid
ω	[rad/sec]	Angular velocity

ANALYSIS OF THE FLOW FIELD
Simplified Model for Analysis

The operational principle of an oval gear flowmeter is shown in Figure 1. One set of the rotors in the housing can be rotated by the pressure difference between the inlet and the outlet. The upper rotor in the perpendicular direction, however, can not exert the rotational driving power due to the symmetry around the rotational centre O. On the other hand, the lower rotor can be rotated counter-clockwise due to the pressure difference (P1 > P2). After this phase of the two rotors, the upper rotor, initially driven by the lower rotor, can also have the clockwise driving torque as shown in Figure 1.

The fluid filled with the crescent-like volume consisted of the lower part of the rotor and housing is discharged two times from the volume during one revolution. Therefore, the total volume passed will be four times of the crescent-like volume, when considering the upper and lower rotors discharge two times of the volume per one revolution. Hence we can find the flow rate only by measuring the number of the revolution.

Although previous studies for turbo-machineries are found to be the prediction of non-contact type seal leakage [4] and the flow analysis of the blade tip clearance [5], the flow field studies of the rotor driven by pressure difference have seldom found yet.
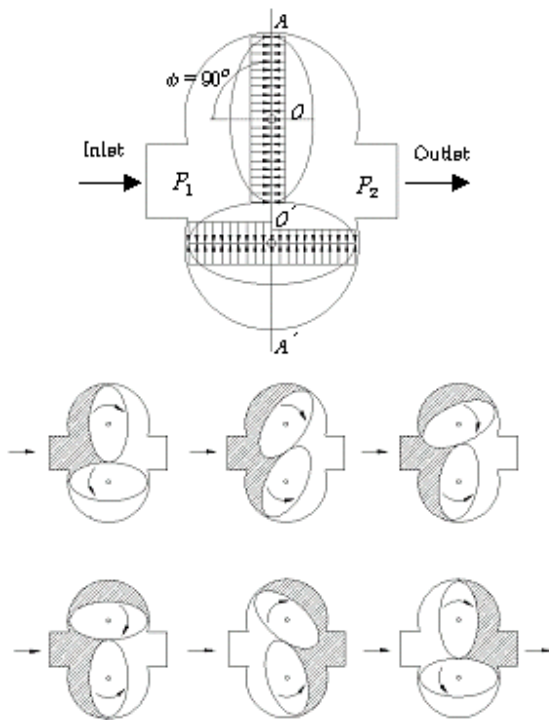

Figure 1 Operating principle

The present model is not the general CFD problem but the coupled fluid and structure one associated with the rotation, movement, and deformation of the structure by fluid. In order to solve the coupled problem, the commercial software ADINA-FSI (Fluid-Structure Interaction) was used. Outline of ADINA-FSI is shown in Figure 2. Various sample solutions using ADINA-FSI are found in Zhang et al.'s paper [6].

The model illustrates the case where there is a flexible solid in the fluid channel. When the fluid passes the solid, the solid may deform due to the interaction with the fluid. The fluid region is defined as the region excluding the solid part. The solid part is the solid region. FSI-interface is defined as the common region where the borders of the solid and the fluid overlap. FSI-analysis introduces the simple assumption that the fluid transmits its own displacement and force to the solid in the same magnitude and direction. In addition, ADINA-FSI has an advantage of generating re-mesh on calculating due to its adoptive mesh function.
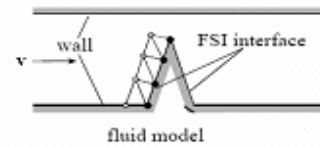
Displacement Compatibility :

$$d_f = d_s \Rightarrow F_f(X_f, X_s) = 0 \qquad (1)$$

(a) Fluid model of FSI
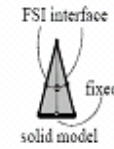
Traction condition :

$$n \cdot \tau_f = n \cdot \tau_s \Rightarrow F_s(X_f, X_s) = 0 \qquad (2)$$

(b) Solid model of FSI

$$F(X) = \begin{bmatrix} F_f^i(X_f, X_s) \\ F_s^i(X_f, X_s) \end{bmatrix} \qquad (3)$$

(c) Equation of FSI

Figure 2 Outline of ADINA-FSI

EXPERIMENT
Flow Visualization

In order to verify the result of flow analysis, flow visualization was performed. In the OG-100K flowmeter, the

opaque base plate is exchanged for a transparent acryl one. The moving picture of the flow field in the housing was taken after the dye from the inlet of the housing is mixed with the water.
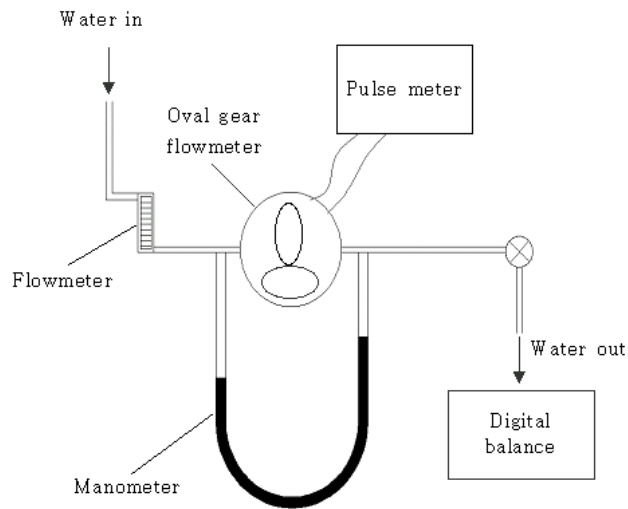

Figure 3 Schematic diagram of experimental apparatus
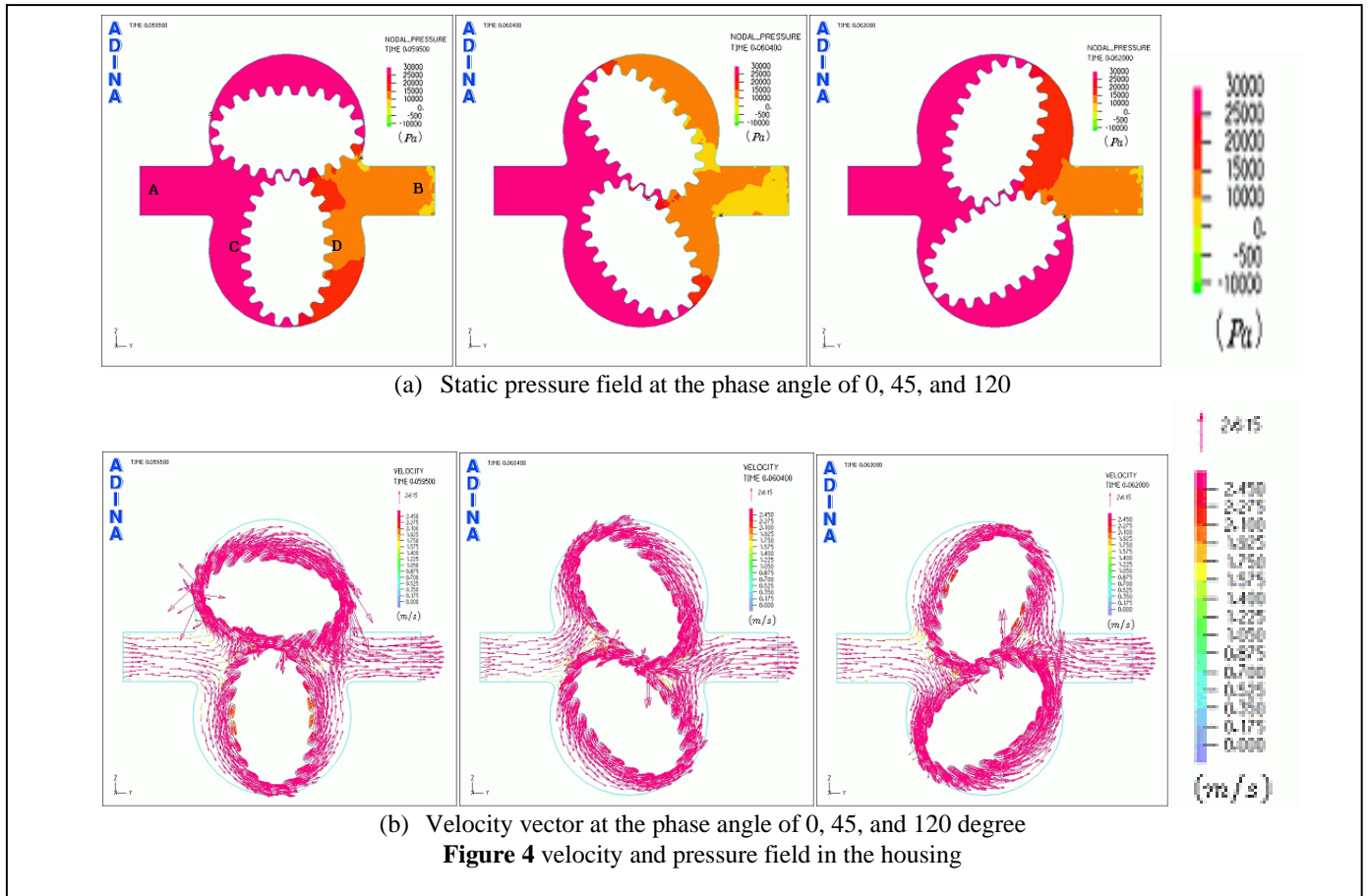
Flowmeter Experiment

Figure 3 shows experimental apparatus with the oval gear flowmeter and some measuring instruments. Ordinary tap water was used for this experiment. For the purpose of adjusting the constant flow rate, an instant flowmeter of Model DYL-375 was inserted in the upstream side of the flowmeter and has ability to adjust the flow rate ranging from 2 to 20 litre/min. In order to measure the number of revolution (rpm) for the rotor, a pulse counter of model FX4Y-I was used. The rpm was calculated from both the number of the pulse and the measuring time for the pulse. The trends of the pulse per litre (ppl) were found from the total fluid weight indicated by digital balance, the rpm, and the measuring time for each measurement. In order to examine the trends of pressure difference between the inlet and the outlet, a mercury manometer was connected to the inlet and outlet, as shown in Figure 3.

RESULTS AND DISCUSSIONS
Results of FSI Analysis

Figure 4 represents the velocity and pressure field with respect to the phase angles (0, 45, 120 degree) of the upper rotor. In connection with Figure 4, Figure 5 represents the long and the short tip velocity variations of the bottom rotor as a function of time, and Figure 6 shows the pressure variations for the points A-D as shown in Figure 4, with respect to time. The point C and D represent the end points of the short axis of the bottom rotor, respectively. In Figure 6, the line-A represents the given inlet pressures (10, 20, and 30 kPa) as a step function of
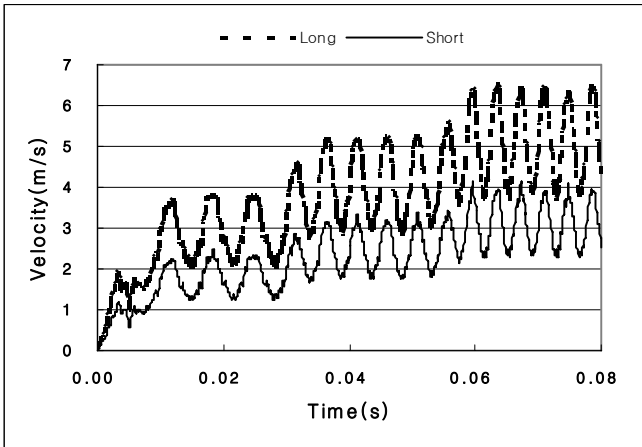

(a) Static pressure field at the phase angle of 0, 45, and 120

(b) Velocity vector at the phase angle of 0, 45, and 120 degree
Figure 4 velocity and pressure field in the housing

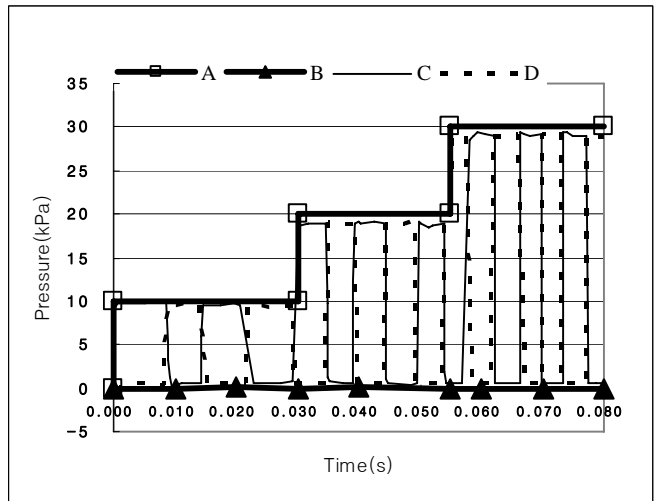**Figure 5** The long and short tip velocities of the bottom rotor.

Figure 6 Pressure variations for A-D points.

time and the line-B denotes the given outlet pressure (0 kPa).

The time period related with the rotor phase angle ranging from 0 to 180 degree, shown in Figure 4 and also in Figure 5, ranges from 0.0595 to 0.0635 second. During this time period, the pressure at the point C has the range from 30 kPa to 0 kPa as shown in Figure 6, and the velocity at the point C has the range from 4.1 to 2.3 m/sec as shown in Figure 5. Simple estimation of the averaged rotor angular velocity leads to 7500 rpm: (Averaged rotor angular velocity) = (0.5 rev.) / (0.004 sec.) = 125 rev/sec = 7500 rpm. Consequently, averaged rotor velocity of the long axis is about 5 m/sec: (Averaged rotor velocity of the long axis) = (12.35 mm /2) (2π) (7500 rpm / 60 sec.) = 5 m/sec. This averaged velocity is the same as that of the long axis located in the range of the time interval from 0.055 to 0.08 second, as shown in Figure 5. Through the similar estimating procedure of rpm and the averaged long axis tip velocity, we can predict the other two values of those for the inlet pressures of 20 kPa and 10 kPa, and can confirm these with the averaged long axis tip velocities (4 m/sec and 3 m/sec, respectively) in Figure 5.

The pressure at point C varies periodically as shown in Figure 4(a) and Figure 6. So does the pressure at point D with the phase shift angle of 180 degree. As mentioned previously, pressure difference around the upper rotor at the phase angle of 0 degree generates the driving torque. And then, the upper and lower rotors have the same magnitude of driving torque at the phase angle of 45 degree. At the phase angle of 120 degree, the lower rotor exerts much greater driving torque.

With examining the velocity field in Figure 4, the fluid enters into the upper and the lower rotor by turns. As a whole, the moving rotor surfaces have higher velocity and the regions in the neighbourhood of the fixed wall and the housing surface have lower velocity. Low velocity regions also exist in wider flow passages, vortex generating areas such as just forward and backward regions of the contact point of the rotors in the phase angle of 45 degree, and just exit region of downstream in that of 45 degree. Higher velocities are also found in narrower flow passages. The highest velocity is located in the long axis tip of the rotor, but the tip velocity varies periodically due to variations of driving torque caused by variations of pressure difference around the rotor, as seen in Figure 5.

Results of Flow Field Visualization

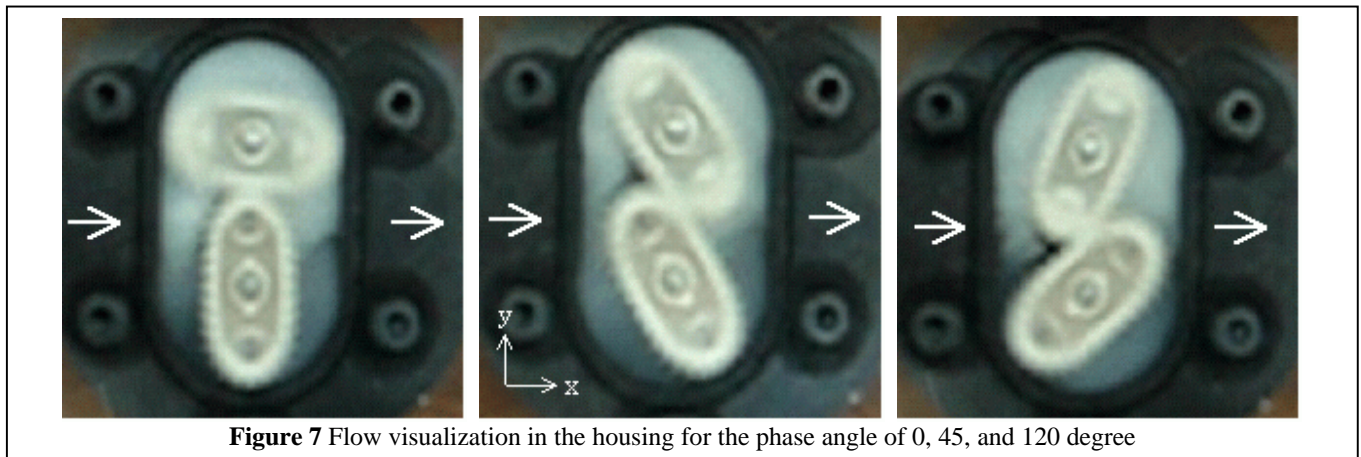In order to verify the results of the present FSI analysis,

Figure 7 Flow visualization in the housing for the phase angle of 0, 45, and 120 degree

flow visualization in the housing of the OG-100K flowmeter was performed. As can be seen in Figure 7, the inlet flow enters into the upper and the lower part of the housing by turns, the same phenomena as observed in the results of the present FSI analysis. In similar manner, the outlet flow and the generated vortices and wakes are discharged by turns from the two rotor surfaces. This can be due to the fact that the rotation of the rotors makes the flow passages to be wider or narrower depending on the geometric features of flow passages from the inlet and outlet rotor arrangements and also the flow to be curvy, to separate (just the upstream side of the gear contact point), and to put together and to split (just the downstream side of the gear contact point).

However, in this experiment, three dimensional flows were observed: A part of upstream based on the contact line of the two rotors enter three-dimensionally into the top and bottom sides of the rotors and then the vortices generated by the top and bottom side rotation of the rotors are mixed with the main downstream.

Results of Flowmeter Experiment

In a gear type flowmeter, the precision is usually represented as ppl (pulse per litre) and its percent. We can estimate the size of the housing and the oval gear from the ppl. For example, with assuming that only one pulse per revolution is detected for an oval gear flowmeter, the flowmeter with the 400 ppl has the discharge rate of 2.5 cc/rev. (Discharge rate per revolution) = (1/400) = 2.5 cc/rev. As the flowmeter discharges four times of the crescent-like volume formed by the housing and the oval gear, the crescent-like volume is 0.625 cc. In addition, maximum and minimum values of rpm can also be estimated from the given measuring range of flow rate. Supposing the same flowmeter with the measuring range from 0.5 to 10 litre/min, the rpm range is from 200 to 4000 rpm, from the fact that (rpm) = (flow rate, litre/min) (ppl). Generally, the oval gear type flowmeter has the precision of $\pm$ 1% at water and $\pm$ 0.5% at 30 cSt oil [7].

In Figure 8, the pressure difference between the inlet and outlet varies from 1 to 30 kPa. The %Error indicating the ratio of ppl at a specific flow rate to the overall averaged ppl for the range of measuring flow rate shows the precision of within 1%. Figure 9 shows the nearly constant value of the ppl (about 46.5 ppl) measured three times for the OG-100K flowmeter, with respect to the flow rate ranging from 2 to 20 litre/min.

At this moment it can be a meaningful work to evaluate approximately the portion of the rotor driving power among the maximum theoretical power supplied by the pressure difference between the inlet and the outlet of the housing. For an incompressible fluid, the maximum power can be given by enthalpy difference between the inlet and the outlet, namely expressed as equation (4), from Bernoulli equation. With assuming that the uniform pressure acting on the rotor (Figure 10(a)), the simplified actual power to drive the rotor can be expressed with the torque and angular velocity, as equation (5). However, actual pressure acts perpendicularly on the elliptical rotor surface. Detailed pressure distributions on the rotor surface are shown in Figure 10(b). In comparison with the two cases in Figure 10, the modified actual power can be written as

equation (6). For two cases of the flow rate (2, 20 litre/min), given geometries and experimental results are shown in Table 1, and then the maximum theoretical power by equation (4) and the modified actual power by equation (6) are presented in Table 2. As a result, for the two cases of the flow rate, power losses of 51.8% and 55.09% represent the purely dissipated portions of the maximum theoretical powers without any contribution to drive the rotors. These may be due to shear work interacted with solid surfaces or between fluid layers, additional energy loss by contraction and enlargement of fluid area, and vortex generation and disappearance by the rotation of the rotors. The portion of the modified actual driving powers of 49.2% and 44.91% were used to drive rotors, and thus were dissipated by the lubrication between the rotor axis and its housings, and finally to increase the internal energy in the flowmeter.
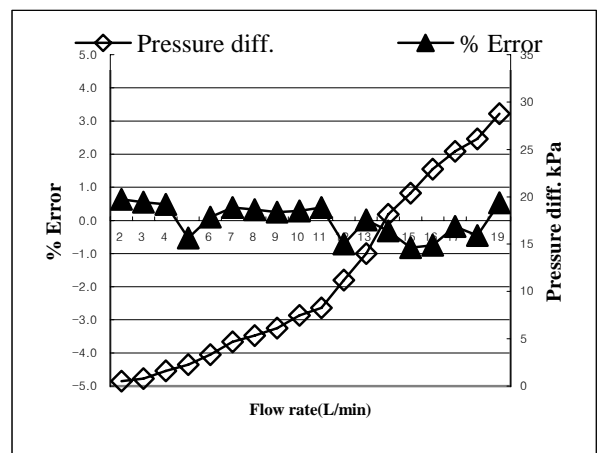

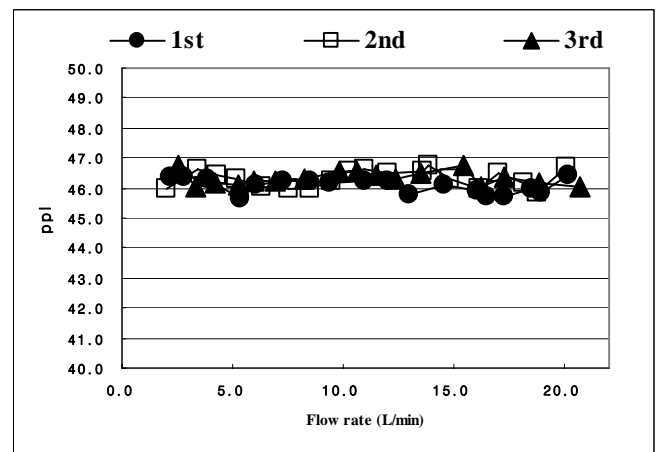**Figure 8** Pressure difference and the relative flow rate error for the OG-100K flowmeter.

Figure 9 ppl variations of the OG-100K flowmeter.

Table 1 Parameters for calculation

Q (L/min)	rpm	ΔP (kPa)	R (m)	A (m2)

| 2 | 100 | 0.5 | 8.75 | 332.5 |
| 20 | 936 | 28 | x 10^{-3} | x 10^{-6} |

Table 2 Calculation results

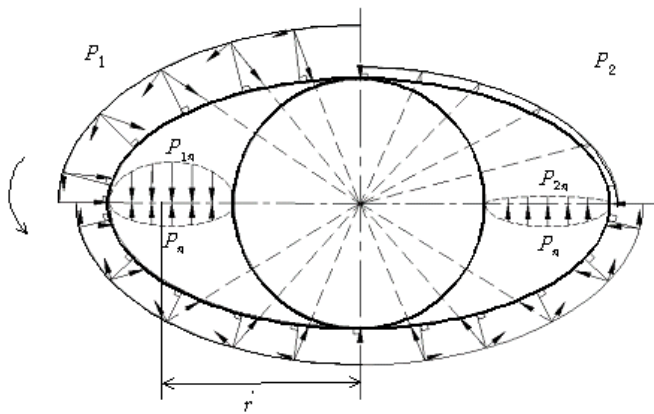| Q (L/min)	$\dot{W}_P$	$\dot{W}_{RM}$	Power loss (%)
2	0.0166	0.008	51.8
20	9.33	4.19	55.09

$$\dot{W}_P = \dot{m}\left(\frac{\Delta P}{\rho}\right) \quad \text{[Watt]} \tag{4}$$

$$\dot{W}_R = T\omega = rF\omega \quad \text{[Watt]} \tag{5}$$

$$\dot{W}_{RM} = \left(\frac{3}{2}r\right)(0.7\Delta P\frac{A}{2})\omega \quad \text{[Watt]} \tag{6}$$
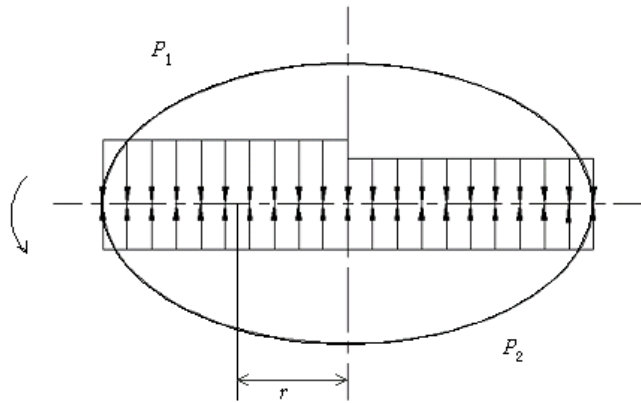
(a) Simplified pressure distribution

(b) Detailed pressure distribution

Figure 10 Pressure distributions around rotor for the phase angle of 0 degree.

CONCLUSION

In an oval gear flowmeter, precision of flow rate is mainly related with the rpm of rotor. The pertinent clearance between rotor and stationary part is trade-off. If too tight, precise rpm may not be generated due to the interference. On the contrary, if too large, leakage flow reduces the precision. For a given rotor and housing geometry and pressure difference, operating characteristics including rpm, average angular velocity, maximum and minimum values of the oscillating rotor tip velocity, was made clear by investigating the pressure and velocity field to rotation angles and their variations with respect to time. The present FSI analysis for the flow field of an oval gear flowmeter indicates that there are periodical variations of the angular velocity and the pressure at a point of rotor.

In flow visualization of the actual flowmeter, similar phenomena of flow field was observed but secondary flow caused by the three dimensional top and surface rotation of the rotor was also observed. This secondary flow makes additional contributions to pressure drop in the housing.

Through the actual flowmeter experiment, the trends of the present FSI analysis were verified. Pressure drop was increased as the flow rate was increased. The ppl and its relative error were found to be 46.5 ppl and less than 1% for water, within a tolerable error in comparison with ordinary oval gear flowmeter.

In connection between the driving power of the rotor and the maximum theoretical power by the pressure difference, somewhat rough estimation of the driving power gives information that nearly 50% of the given theoretical power was converted into the driving power and the remaining part was dissipated into the fluid inside of the housing. Higher flow rate results in higher portion of power loss.

REFERENCES

[1] Lim, K.W., and Cha, D.-J., An experiment study on the characteristics of oval gear flowmeter, *Research Journal in Research Center Based on Production at Hanbat Nat'l Univ.,* Vol. 2, No. 1, 2002, pp.158-166.

[2] Litvin, F. L., *Gear Geometry and Applied Theory*, University of Illinois at Chicago, 1994, pp. 347-381.

[3] Ko, Y. H., and Choi, S. H., A study on the design of elliptic non-circular (Lobe Type) gears, *Autumn Conference of KSPE 1994*, 1994, pp. 622- 626.

[4] Ha, T. W., Prediction of non-contact type seal leakage using CFD, *Journal of KFMA,* Vol. 9, No. 3, 2006, pp. 14-21.

[5] Ro, S. H., Numerical analysis on the blade tip clearance flow in the axial rotor (Ⅱ), *Trans. of the KSME (B)*, Vol. 23, No. 9, 1999, pp. 1106-1112.

[6] Zhang, H., Zhang, X., Ji, S., Guo, Y., Ledezma, G., Elabbasi, N., and deCougny, H., Recent development of fluid-structure interaction capabilities in the ADINA system, *Computers & Structures,* Vol. 81, 2003, pp. 1071-1085.

[7] Some catalogues from manufacturers including Omega Ltd.